Supplementary Information

Two-photon comb with wavelength conversion and 20-km distribution for quantum communication

Supplementary note 1: Quantum state tomography

As described in the manuscript, we measured two-photon coincidence counts in 16 polarization basis. This follows Ref. [1] and demands only one waveplate rotation between each measurement, shortening the total measurement time. **Supplementary Figure 1** shows coincidence counts for the Bell states $|\Psi^{+}\rangle$ and $|\Psi^{-}\rangle$, which are realized by installing 45° slow-axis half-wave plate without yaw angle and 0° slow-axis half-wave plate with a yaw angle. The apparent difference appears in the counts for n10 ($|\mathrm{DD}\rangle$) and n16 ($|\mathrm{RL}\rangle$): By changing the yaw angle of only one half-wave plate, these counts visibly increase and decrease. Because of this advantageous nature, we could achieve high fidelity and arbitral relative-phase adjustment. The counts for $|\Psi^{-}\rangle$ is a slightly low because of the misalignment of the optical path due to larger yaw angle.

Tomographic reconstruction and maximum likelihood method are achieved based on Ref. [2], which is an available program in Git Hub; thus, there is no room for our conveniences or mistakes in tomography experiment. Furthermore, to depict the density matrix, QuTiP library in python is used [3]. In this whole processing, fidelity is defined as $\mathcal{F} = \langle \phi_{ideal} | \rho_{reconstruct} | \phi_{ideal} \rangle$, which is a common definition (however, this is not square-root fidelity [4]). For further higher fidelity, improvement of the basin-like structure, which appears small in n16 count (left side of **Supplementary Figure 1**), is required. This is caused by polarization rotating along cavity-round-trip phase shift by passing through crystals or reflection on dielectric mirror with a few angles; it can be reduced by finely adjusting the crystal position and decreasing the reflection angle.

Our main effort aiming at high fidelity is to reduce decoherence effect as much as possible. We construct a bow-tie cavity with a small reflection angle (approximately 2-3 degrees) to decrease senkrecht and parallel polarization dependence. This angle is limited by finite width of PPLN crystal; the minimum magnitude is proportional to arctangent of the half of the short arm of bow-tie configuration and the width of PPLN. Long cavity can make reflection angle smaller than ordinal-size cavity, resulting in decoherence. Also, a PPLN crystal has birefringence, and we adjust the temperature of two PPLNs with a few milli-kelvin stabilities to reduce total birefringence. Furthermore, the mirrors after the cavity for coupling to the PMF are all removed, and two photons straightly couple into the PMF. These are only a few examples to realize high fidelity: dephasing mechanism is very complex in reality.

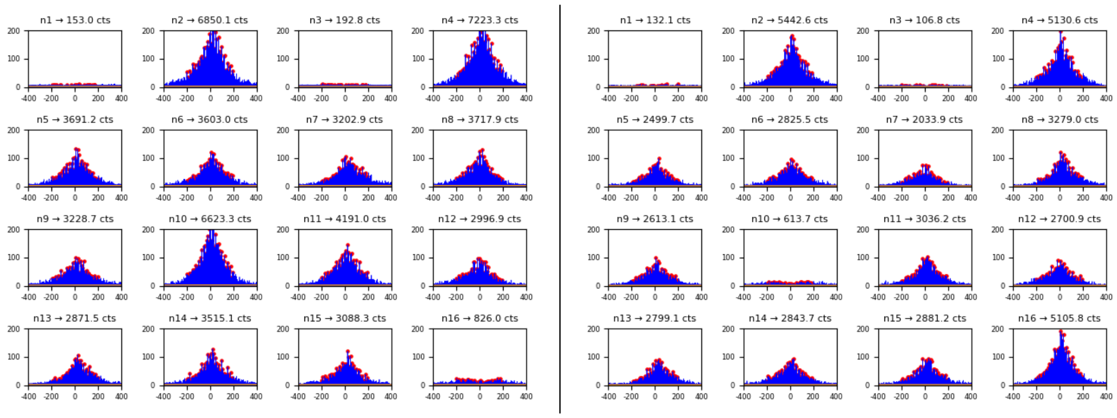

Supplementary Figure 1. Two examples of coincidence count in 16 measurements, on the $|\mathrm{HH}\rangle, |\mathrm{HV}\rangle, |\mathrm{VV}\rangle, |\mathrm{VH}\rangle, |\mathrm{RH}\rangle, |\mathrm{RV}\rangle, |\mathrm{DV}\rangle, |\mathrm{DH}\rangle, |\mathrm{DR}\rangle, |\mathrm{DD}\rangle, |\mathrm{RD}\rangle, |\mathrm{HD}\rangle, |\mathrm{VD}\rangle, |\mathrm{VL}\rangle, |\mathrm{HL}\rangle, |\mathrm{RL}\rangle$ basis. Left (right) is the case of generating Bell state of $|\Psi^{+}\rangle$ ($|\Psi^{-}\rangle$). Blue represents raw counts and red represents counts within a range of [-200, 200] ns. SPDC pump light is nearly $|D\rangle$ polarized with a power of 100 μW. Each acquisition time is 15 s, and the total time becomes about 10 min due to waveplate rotation. The only difference between these two experiments is the yaw angle of the half-wave plates.

Supplementary note 2: Dependence of two-photon coincidences on SPDC pump power

We demonstrated that $g_{s,i}^{(2)}(0)$ of WC-TPC can overcome that of original TPC (Fig. 4 (b)). In this supplementary note, we focus on original TPC or telecom two-photon correlation before WC. **Supplementary Figure 2** (a) shows two-photon timing correlation with the conditions of SPDC-pump power of 10 mW, polarization of only $|H\rangle$, SSPD detection efficiency of ~ 60%, and bin size corresponding to the resolution of 16 ps. Noise slope can be observed at the right side in this figure, which continues to plummet which very rapidly reach the zero count. This is natural for the case of high-count range at nearly 10 MHz because coincident detection occurs in the vicinity of zero. Although this noise curve must have continued toward the left (minus of time axis), it appears flat for some range. This results from the dead time ~ 80 ns of our time-correlated single photon counting module HydraHarp 400. Without dead time, the whole noise function would become a slope and $g_{s,i}^{(2)}(0)$ would be different from this data.

Supplementary Figure 2 (b) is a log scaled version of Fig. 4 (b), which is obtained by only changing SPDC pump power (all the other parameters are the same as above). TPC without WC can be observed more clearly with higher $g_{s,i}^{(2)}(0)$ in lower power range. This is because the photon-pair number inside a cavity becomes lower and the noise caused in the crystal approaches zero. This function must converge to 1 at very low pump power because no pump would cause only dark counts; however, we have never observed this point because our SSPD has excellent-low noise count (in the order of 10 cps). In the low power range, the gradient in the logarithmic graph shows almost -1 resulting in inversely proportional change to the pump power.

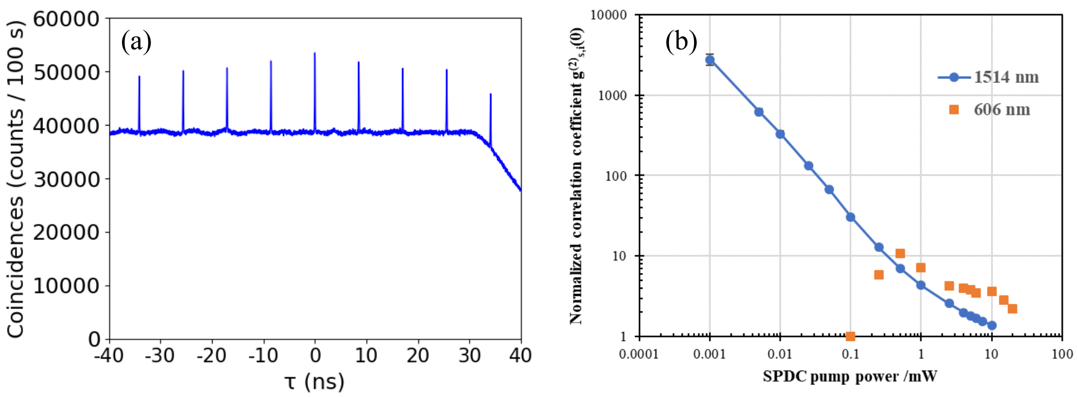

Supplementary Figure 2. Two-photon coincidences focused on SPDC pump power. (a) Coincidence counts of 1514 nm two photons. SPDC pump power is 10 mW, and the detection efficiency of superconducting single photon detector (SSPD) is adjusted as ~ 60% to not reach the maximum rate per channel. (b) Normalized correlation coefficient $g_{s,i}^{(2)}(0)$ versus SPDC pump power (same as Fig. 4 (b) in main article). The blue circles connected by a line represents 1514 nm two photon data (without WC), and the orange squares represent WC-TPC. Although SSPD and silicon avalanche photodiode (SiAPD) have almost the same efficiency of 60% because of regulation of the applied current, the timing jitters differ greatly: ~40 ps for SSPD and ~300 ps for SiAPD.

Supplementary note 3: Estimation of bandwidth of TPC spectrum

In general, spectrometer or optical grating is widely used to analyze a spectrum. However, these "bandpass method" has a little difficulty of high optical loss. Further, when measuring both two photons, two frequency-correlated setups are required because two photons satisfy energy conservation. Then, we suggest another new method to estimate two-photon spectrum with lower loss and relatively easy setup.

We utilize 10 km single-mode fiber and observe dispersion of TPC. In general, optical fiber has birefringence and the optical path length could change depending on the fiber condition. When only the influence of dispersion is required, a correlation of two photons dispersed in the same fiber is suitable under the approximation that the fiber remains almost unchanged within the coherence time. **Supplementary Figure 3** shows dispersed two-photon correlation after 10 km fiber with an SPDC pump power of 10 μW. These results are obtained due to a long time interval caused by our long cavity. To estimate the timing width, we used the following equations:

$$G_{s,i}^{(2)}(\tau) = c \times e^{-2\pi f_{FWHM}|\tau|} \times \mathrm{Comb}(\tau) + \mathrm{noise}\,,$$

$$\mathrm{Comb}(\tau) = \sum_{n=-(N-1)}^{N-1} \exp\left[-4(\ln 2)\left(\frac{\tau - n t_{FSR}}{T_{FWHM}}\right)^2\right],$$

where c is a coefficient corresponding to peak counts; f_{FWHM} represents full width at half maximum (FWHM) of one frequency peak, i.e., linewidth; N is related to the number of timing combs; t_{FSR} denotes the time interval expressed as a reciprocal of free spectral range (FSR); T_{FWHM} is the FWHM of one timing peak which is approximated by a Gaussian-shape peak. Although a Voigt function should be used for the strict estimation of the spectrum, we used a Gaussian function to reduce complexity. The red line corresponds to this function; although it appears smaller than raw data, the insets show that it has some variance around the peak counts. From this figure, despite passing through the 10 km fiber, frequency linewidth f_{FWHM} is almost the same as that of ~1.35 MHz that corresponds to 95% reflectivity of cavity output coupler. T_{FWHM} is 2.0 ± 0.2 ns ns from (a) and 4.0 ± 0.3 ns from (b) among 10 peaks. The timing jitter of our measurement system is ~0.1 ns, and has ignorable influence on these values. The dispersion value around 1514 nm can be calculated using the dispersion equation as ~+15 ps·nm^{-1}·km^{-1}; then, we estimate the TPC frequency bandwidth of ~13 nm.

Such a very long timing can be compensated using a special fiber having an opposite sign of dispersion value. If this compensation can be considered as one of the re-modulations of wave packet, it can recover the quantum coherence as well [6]. Moreover, using band-pass effects such as WC, we can eliminate this broadening (Fig. 4 (c) in main text).

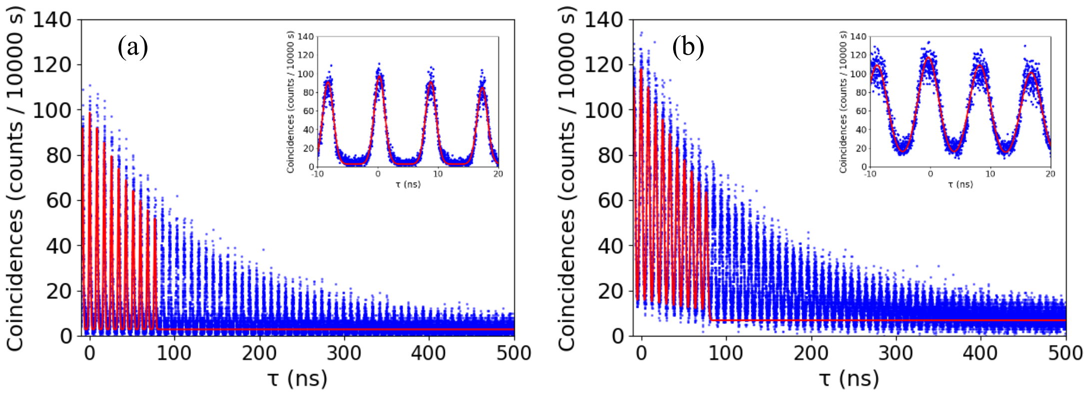

Supplementary Figure 3. Two-photon coincidence counts with dispersion after passing through the 10 km optical fiber: (a) only one photon and (b) two photons. Blue represents raw data point and red represents the fitted function (only 10 pieces of gaussians are pictured). Insets are the enlargements of the regions around the center $\tau = 0$.

Supplementary note 4: The efficiency and noise of wavelength converter

The main characteristics of a wavelength converter are the quantum efficiency of conversion and the counts of noise. Quantum efficiency is calculated as follows [7]:

$$\eta = \frac{N_{converted}}{N_{telecom}} = \frac{P_{convered}/h\nu_{converted}}{P_{telecom}/h\nu_{telecom}} = \sin^2\left(L\sqrt{\eta_{nor}P_{pump}}\right),$$

where N, P, ν, L, η_{nor}, and P_{pump} represent the number of photons, power of light, frequency of light, length of wavelength-conversion crystal, normalized power efficiency in the low-gain limit, and pump power, respectively. We used a 48 mm PPLN waveguide with a cross section of $9.9\ \mu\mathrm{m} \times 11.5\ \mu\mathrm{m}$ to realize higher efficiency than bulk.

Supplementary Figure 4 (a) shows a quantum efficiency η. We used telecom laser to directly measure the external efficiency, which is the conversion efficiency, including waveguide-coupling efficiency and transmission loss, but removed the influence of the auxiliary laser. Further, we obtained the telecom-laser coupling rate by turning the WC pump laser off, to estimate the internal efficiency. The maximum external efficiency we could measure was 56.0%; however, it appears to increase slightly at higher pump power range. The coupling rates at 1514 nm and 1010 nm are 59.4% and 60.5%, respectively; then, we can estimate the internal efficiency. Our crystal is designed to have an efficiency of nearly 1, and the measured maximum value was 94.3%.

Noise count is obtained as shown in **Supplementary Figure 4** (b). In this measurement, only WC pump laser is used, and the filters consist of two dichroic mirrors and one bandpass filter. The dotted curve represents quadratic-function fitting and the measured data set are almost positioned on fitting. This indicates that noise is mainly caused by second-order nonlinear optical process in this setup. Then, we analyze the component noise spectrum using a spectrometer. The result indicates one peak, which is centered on 606 nm and a FWHM of ~ 25 GHz (not shown). We then try to adjust the number of filters or optical depth by adopting other bandpass filters or filtering crystals.

In **Supplementary Figure 5**, we defined the wavelength-conversion function η^* as the ratio of external efficiency and noise rate at kilo counts per second. In this process, the approximated function η and the quadratic noise function are used. This function has no meaning in absolute value because of strange unit (% divided by kilo counts), but indicates the pump-dependent signal-to-noise ratio. This calculation is similar to reference [8]. The maximum point is positioned at 7.97 mW pump power in our condition of dark counts of ~0.32 kHz; on using lower dark counts, this point shifts toward the left. Although this pump power was the best to obtain high SNR, we chose a higher power of 50 mW to obtain shorter experimental time for accurate comparison of $g_{s,i}^{(2)}(0)$ (**Supplementary Figure 2** (b)). As one of the indices, noise equivalent power (NEP) is often adopted [9], and the optimum pump power of that shows 46.8 mW. The actual comparison of the two-photon coincidences is shown in the next supplementary note.

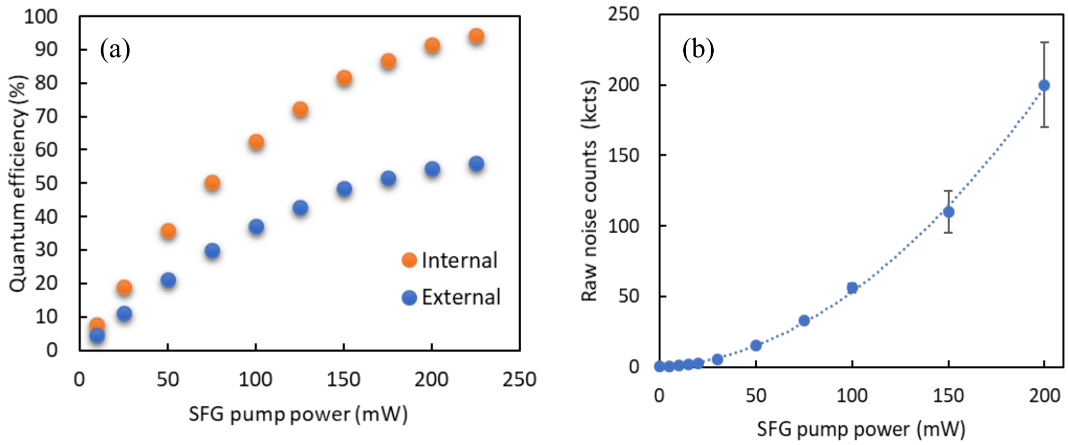

Supplementary Figure 4. Specifications of wavelength converter. (a) Conversion efficiency, defined as the ratio of the number of photons before and after WC. (b) Raw noise counts obtained by inputting only 1010 nm auxiliary laser and installing two dichroic mirrors and one bandpass filter.

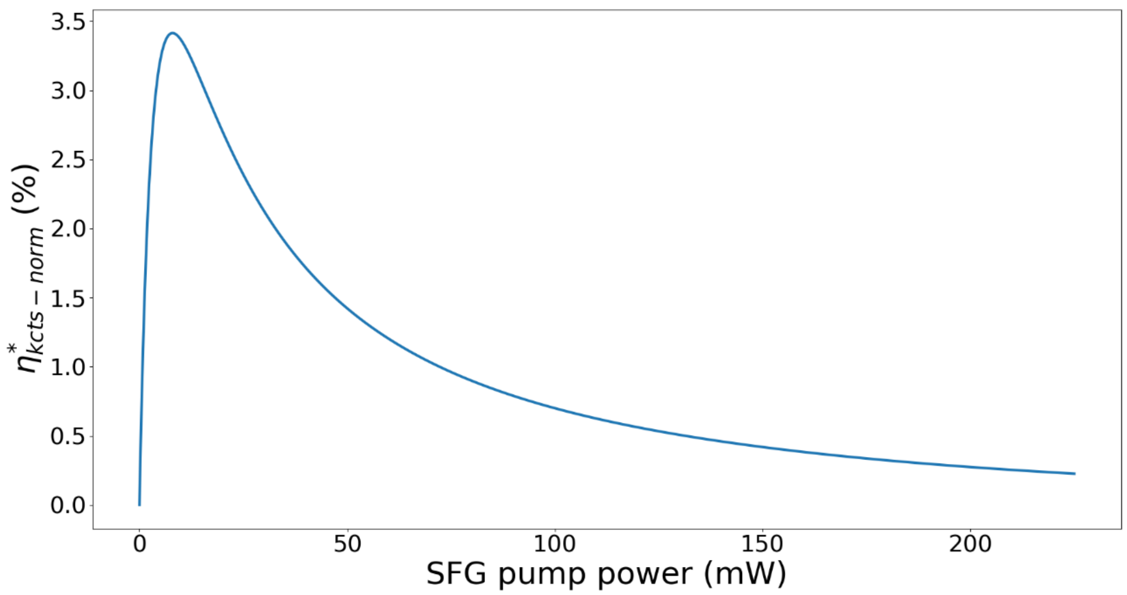

Supplementary Figure 5. Noise-normalized conversion efficiency η^*, which we defined as the external efficiency curve divided by the noise count curve of kilo counts per second. The peak can be realized at the SFG pump power of 7.97 mW. This value is strongly influenced by the dark count rate.

Supplementary note 5: Dependence of WC-TPC on auxiliary laser power

This note is related to wavelength conversion efficiency and noise count. In the previous section, we demonstrated that a trade-off exists between them, and we had to search for a balanced pump power of WC. **Supplementary Figure 6** shows pump-power dependent $G_{s,i}^{(2)}(0)$ of WC-TPC with SPDC pump power of 5 mW. The values in the figure correspond to external conversion efficiency and noise level (raw count rate, i.e., SPD detection rate after passing filters and coupled to single-mode fiber without beam splitter). Because the heights of peak are arranged to almost same among the figures, the noise floors correspond to normalized correlation functions $g_{s,i}^{(2)}(0)$. These three functions indicate that lower pump power corresponds to better SNR. In our setup, telecom two photons, whose counts are stabilized within 10% of the accumulating time, are transmitted through a polarization-maintaining fiber; therefore, converted photons must be of almost the same number. Further, the main reason is the increase in noise count with the increasing pump power.

We compare **Supplementary Figure 7** (a) and (b) to perform WC-TPC with lower pump power: (a) is the case of very weak SPDC pump of $100\ \mu W$ and WC pump of 10 mW, whereas (b) has the same SPDC pump but a WC pump of 50 mW. There is a clear difference in $g_{s,i}^{(2)}(0)$, but the coincidence rate of (a) is very low at ~0.1 cts/sec (3000 cts/30000 sec).

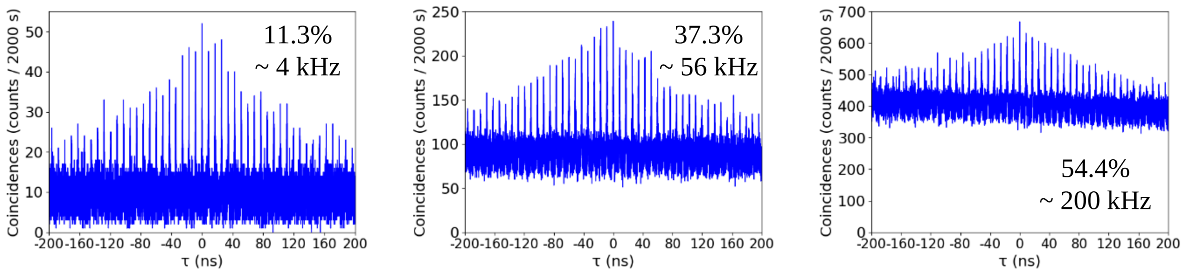

Supplementary Figure 6. WC-TPC at various WC pump powers of 25 mW, 100 mW, and 200 mW. These all are used 5-mW SPDC pump power. The values shown inside the plots are external quantum efficiency (top) (%) and noise count rate (bottom) (kHz).

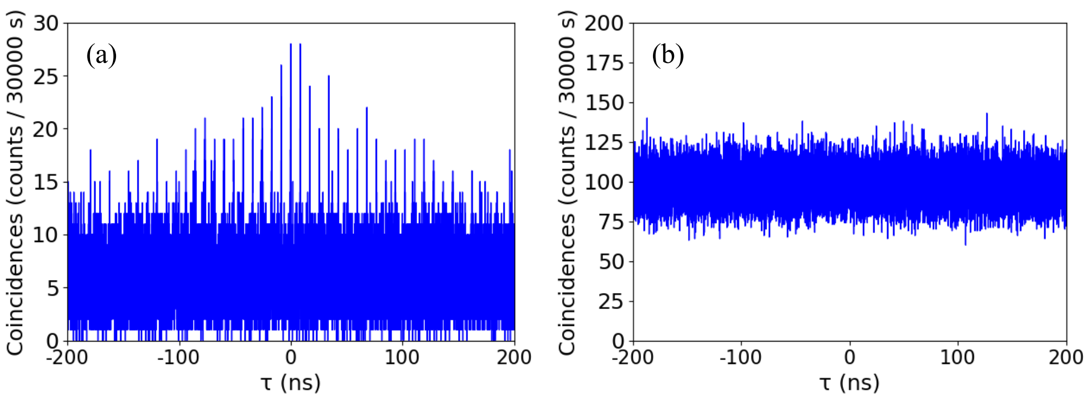

Supplementary Figure 7. (a) WC-TPC with relatively weak lasers. SPDC pump is $100\ \mu W$ and WC pump is 10 mW. At higher WC pump power, this structure cannot be realized because of noise. (b) Same SPDC pump as in (a) but WC pump of 50 mW.

Supplementary note 6: Comparison with previous studies on narrow-linewidth photon sources

It must be beneficial to compare with previous researches. We would like to emphasize that there is no demonstration of telecom narrow-linewidth entanglement source. **Supplementary Table 1** lists some excellent photon sources with narrow linewidth. Although it requires spectral brightness to evaluate the photon source, a more important index is the operational photon-generation rate, which can be enhanced by increasing the pump power up to the parametric threshold. Ref. [15] performed multi-mode polarization-entanglement state tomography; however, it indicates approximately 10% worse fidelity than the single-mode case. This shows a possibility that our photon source can realize higher fidelity with a fewer number of modes. Furthermore, narrower linewidth corresponds to longer coherence time; thus, realizing high fidelity becomes difficult because a wider timing window is required, resulting in decreased fidelity in accordance with the imperfection of experiment like instability or accidental coincidences [6]. The TPC setup is suitable to overcome degradation of quality caused by experimental imperfections and long time passing, for instance, maintaining a sufficiently narrow linewidth and realizing high fidelity.

1st Author (Year)	Characteristics	λ (nm)	$\Delta\nu$ (MHz)	Fidelity (%)	Mode
[10] J. Fekete (2013)	One wavelength aims at direct absorption of Pr^{3+}:YSO	1436 606	1.7, 2.9	-	1
[11] Z. -Y. Zhou (2014)	Telecom	1560	8	-	Multi
[12] K. Liao (2014)	Four wave mixing using ^{85}Rb with magneto-optical trap	780 795	0.8	95.2	1
[13] L. Tian (2016)	Single Mode (Degenerate SPDC)	795	15	95.2±0.8	1
[14] M. Rambach (2016)	Flip-trick technique to realize very narrow linewidth	795	0.67*	-	Multi
[15] J. Wang (2018)	Alignment using optical wedges	935 880	9, 9.5	89.6 (~80)	1 (Multi)
This work	**Telecom narrow linewidth and entanglement with frequency multimode**	**1514**	**0.95**	**96.1**	**Multi**

Supplementary Table 1. List of photon sources. Although numerous photon sources have been developed to date [16], only a few examples were given from the standpoint of outstanding value. * this value indicates the cavity damping rate, although they assert that the actual linewidth of photon (or 1 mode) must be 0.64 times smaller than the damping rate.

Supplementary note 7: Atomic frequency comb quantum memory

This note supplies the outline of atomic frequency comb (AFC) quantum memory scheme using Pr^{3+}:YSO [17]. Pr^{3+} is the dopant of YSO crystal and the concentration corresponds to replacement percentage of Y atom with Pr^{3+} ion. Then individual Pr^{3+} ion possesses specific absorption line around ~ 494.7 THz or 606 nm because of surrounding environment or crystal field. As a whole ensemble, this crystal looks having wide-broadened absorption line, as named, inhomogeneous broadening (see **Supplementary Figure 8** right). Inhomogeneous broadening has a width of the order of from GHz to hundred GHz depending on dopant concentration. AFC structure is tailored into inhomogeneous broadening within a range of < 4 MHz, the width of < 100 kHz, and the comb separation of ~ 100 kHz (this separation is directly related to rephasing time or photon echo time). For instance, the width of (36±3) kHz and comb separation of approximately 137 kHz are used [18]. This comb structure can be established thanks to hyperfine structure (see **Supplementary Figure 8** left) and the long lifetime of that. Because AFC structure is some-order narrower than inhomogeneous width, we can tailor many AFC structure [19][20] with separation of ~ 120 MHz, which corresponds to the FSR of present two-photon spectrum (**Supplementary Figure 9**). Our wavelength converter has bandwidth of 25 GHz and it just fits to inhomogeneous width of 1-100 GHz. On the other hand, our (telecom) TPC has ~1-THz overall bandwidth and if it becomes necessary to use more than 25 GHz for more frequency multiplexing, wider bandwidth wavelength converter is required.

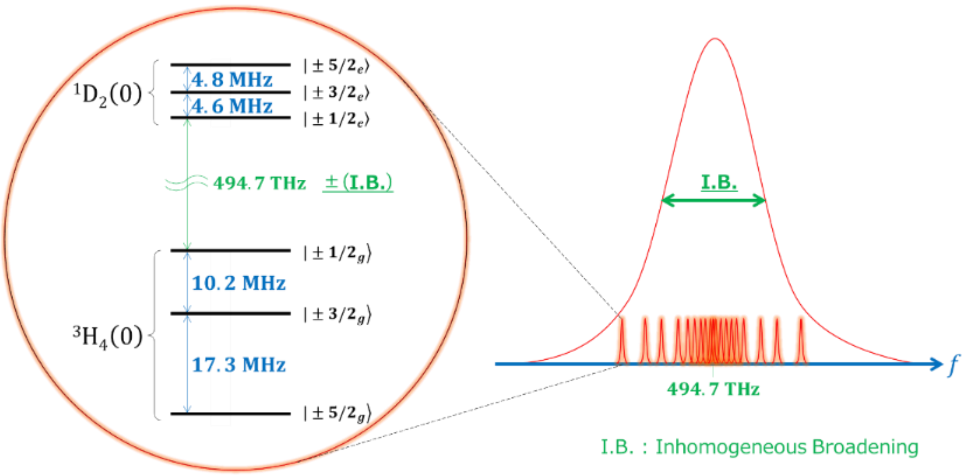

Supplementary Figure 8. Energy diagram (left) and inhomogeneous broadening (right) of Pr^{3+}:YSO.

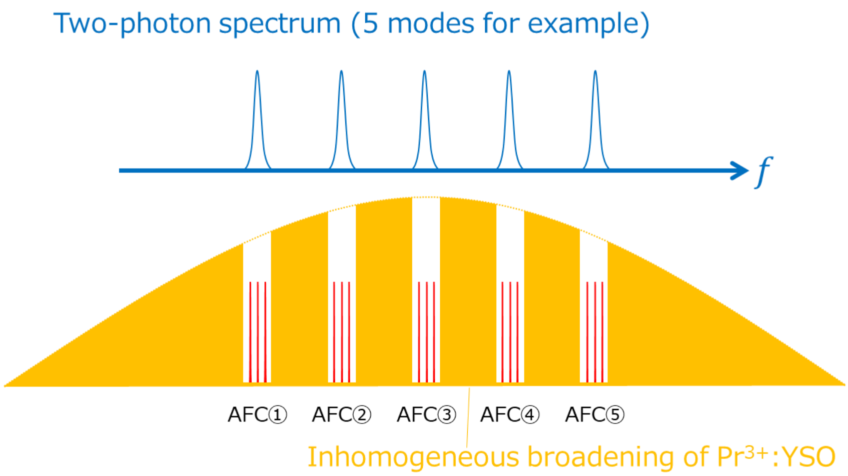

Supplementary Figure 9. AFC structure for frequency multimode.

Supplementary References

[1] James, D. F. V., Kwiat, P. G., Munro, W. J. and White, A. G. Measurement of qubits. Phys. Rev. A **64**, 052312 (2001).

[2] Fokkens, T., Fognini, A. and Zwiller, V. Optical Quantum Tomography Code. Available at https://github.com/afognini/Tomography/ .

[3] Johansson, J. R., Nation, P. D. and Nori, F. QuTiP: An open-source Python framework for the dynamics of open quantum systems. Comp. Phys. Comm. **183**, 1760-1772 (2012).

[4] Altepeter, J. B., Jeffrey, E. R. and Kwiat, P. G. Photonic State Tomography. Advances In Atomic, Molecular, and Optical Physics **52**, 105-159 (2005). (see note 6)

[5] Goto, H., Yanagihara, Y., Wang, H., Horikiri, T. and Kobayashi, T. Observation of an oscillatory correlation function of multimode two-photon pairs. Phys. Rev. A **68**, 015803 (2003).

[6] Wu, C.-H., Liu, C.-K., Chen, Y.-C. and Chuu, C.-S. Revival of Quantum Interference by Modulating the Biphotons. Phys. Rev. Lett. **123**, 143601 (2019).

[7] Roussev, R. V., Langrock, C., Kurz, J. R. and Fejer, M. M. Periodically poled lithium niobate waveguide sum-frequency generator for efficient single-photon detection at communication wavelengths. Opt. Lett. **29**, 1518-1520 (2004).

[8] Yu, Y. et al. Entanglement of two quantum memories via fibres over dozens of kilometres. Nature **578**, 240–245 (2020).

[9] Langrock, C. et al., Highly efficient single-photon detection at communication wavelengths by use of upconversion in reverse-proton-exchanged periodically poled LiNbO3 waveguides. Opt. Lett., **30**, 1725−1727 (2005).

[10] Fekete, J., Rieländer, D., Cristiani, M. and de Riedmatten, H. Ultranarrow-Band Photon-Pair Source Compatible with Solid State Quantum Memories and Telecommunication Networks. Phys. Rev. Lett. **110**, 220502 (2013).

[11] Zhou, Z.-Y., Ding, D.-S., Li, Y., Wang, F.-Y. and Shi, B.-S. Cavity-enhanced bright photon pairs at telecom wavelengths with a triple-resonance configuration. J. Opt. Soc. Am. B **31**, 128-134 (2014).

[12] Liao, K., Yan, H., He, J., Du, S., Zhang, Z.-M. and Zhu, S.-L. Subnatural-Linewidth Polarization-Entangled Photon Pairs with Controllable Temporal Length. Phys. Rev. Lett. **112**, 243602 (2014).

[13] Tian, L., Li, S., Yuan, H. and Wang, H. Generation of Narrow-Band Polarization-Entangled Photon Pairs at a Rubidium D1 Line. J. Phys. Soc. Jpn. **85**, 124403 (2016).

[14] Rambach, M., Nikolova, A., Weinhold, T. J. and White, A. G. Sub-megahertz linewidth single photon source. APL Photonics **1**, 096101 (2016).

[15] Wang, J. et al. Universal Photonic Quantum Interface for a Quantum Network. Phys. Rev. Appl. **10**, 054036 (2018).

[16] Slattery, O., Ma, L., Zong, K. and Tang, X. Background and Review of Cavity-Enhanced Spontaneous Parametric Down-Conversion. Journal of Research of the National Institute of Standards and Technology **124**, 124019 (2019).

[17] Afzelius, M., Simon, C., de Riedmatten, H. and Gisin, N. Multimode quantum memory based on atomic frequency combs. Phys. Rev. A **79**, 052329 (2009).

[18] Seri, A. et al. Quantum Correlations between Single Telecom Photons and a Multimode On-Demand Solid-State Quantum Memory. Phys. Rev. X **7**, 021028 (2017).

[19] Yang, T.-S. et al. Multiplexed storage and real-time manipulation based on a multiple degree-of-freedom quantum memory. Nat. Commun. **9**, 3407 (2018).

[20] Seri, A. et al. Quantum Storage of Frequency-Multiplexed Heralded Single Photons. Phys. Rev. Lett. **123**, 080502 (2019).